

ChemComm

Accepted Manuscript



This is an *Accepted Manuscript*, which has been through the Royal Society of Chemistry peer review process and has been accepted for publication.

Accepted Manuscripts are published online shortly after acceptance, before technical editing, formatting and proof reading. Using this free service, authors can make their results available to the community, in citable form, before we publish the edited article. We will replace this *Accepted Manuscript* with the edited and formatted *Advance Article* as soon as it is available.

You can find more information about *Accepted Manuscripts* in the [Information for Authors](#).

Please note that technical editing may introduce minor changes to the text and/or graphics, which may alter content. The journal's standard [Terms & Conditions](#) and the [Ethical guidelines](#) still apply. In no event shall the Royal Society of Chemistry be held responsible for any errors or omissions in this *Accepted Manuscript* or any consequences arising from the use of any information it contains.



Journal Name

COMMUNICATION

Mesoporous BaSnO₃ layer based perovskite solar cells

Liangzheng Zhu,^{ab} Zhipeng Shao,^a Jiajiu Ye,^{ab} Xuhui Zhang,^{ab} Xu Pan,^{*a} and Songyuan Dai^{*c}Received 00th January 20xx,
Accepted 00th January 20xx

DOI: 10.1039/x0xx00000x

www.rsc.org/

One of the limitations of TiO₂ based perovskite solar cells is the poor electron mobility of TiO₂. Here, perovskite oxide BaSnO₃ is used as a replacement. It has higher electron mobility and the same perovskite structure as the light harvesting materials. After optimization, devices based on BaSnO₃ gave the best performance of 12.3% vs 11.1% for TiO₂.

Due to their high photovoltaic performance, potential high efficiency and simple procedure to assemble, perovskite solar cells (PSCs) are gaining more and more attention. In 2009, Miyasaka et al.¹ employed CH₃NH₃PbX₃ (X = Br, I) as sensitizer in dye-sensitized solar cells to replace organic dyes. However, CH₃NH₃PbX₃ is not suitable for liquid electrolyte-based devices because of its poor stability in polar solvent. Until 2012, Park and his co-workers first reported a relatively long-term stable all-solid-state PSC with a promising power conversion efficiency (PCE) of 9.7%.² Snaith et al. used Al₂O₃ as mesoporous layer and achieved an excellent efficiency of 10.9%.³ After that, Gratzel et al. developed a novel sequential deposition method for the fabrication of PSCs and attained a PCE of 15%.⁴ Then, PSCs were under intense investigation and great achievements were obtained.⁵⁻¹⁰ Recently, Seok et al. reported an approach for depositing high-quality formamidinium lead iodide (FAPbI₃) films by the direct intramolecular exchange.¹¹ The resulting FAPbI₃ based PSC exhibited an efficiency of over 20%.

There are two branches of PSCs: mesoscopic nanostructure and planar structure.¹² The most widely used mesoporous layer is TiO₂ for its unique chemical and electronic properties and good performance in dye-sensitized solar cells.¹³ The role of mesoporous layer is quite important. It has been proved that

carriers transport through the mesoporous TiO₂ layer is not neglectable.¹⁴ The successful application of Al₂O₃ in PSC³ not only inspired researchers but also challenged them. This proved that carrier transport process can be done by perovskite itself and provides ideas for the emerging planar heterojunction PSC. But it also challenged them why would the carrier transport through TiO₂ with higher priority. Anyway, it verifies the importance of mesoporous layer in PSCs. Other candidates expected to replace TiO₂ were also studied. The successful introduction of Al₂O₃¹⁵ and functionalized silica¹⁶ nanoparticles directly into the perovskite precursor solution to form a co-deposited mesoporous layer made a contribution to the commercialisation and scale-up of PSCs. ZnO has an electron mobility approximately two orders of magnitude higher than TiO₂.¹⁷ Many PSCs based on ZnO nanorods or nanowires were fabricated,^{18,19} because this nanostructure reduces unnecessary path of the charge carrier.²⁰ Effects of the mesoporous layers are highly anticipated, Zn₂SnO₄,²¹⁻²³ SrTiO₃²⁴ and graphene/TiO₂ nanocomposites²⁵ were also used as mesoporous layers in PSC.

BaSnO₃(BSO), a kind of transparent semiconducting perovskite oxide, has a large optical band gap, around 3.1 eV, and a relatively high electron mobility (μ) at room temperature.²⁶ It is quite easy to modify its electronic or optical properties by manipulating the composition or doping. One of the limitations of TiO₂ based PSCs is the comparatively low electron mobility of TiO₂.¹² However, La-doped BSO single crystals and epitaxial thin films show unprecedentedly high μ values about 320 cm² V⁻¹ s⁻¹ and 70 cm² V⁻¹ s⁻¹, respectively. Because of the advantages mentioned above, BSO was already applied in dye-sensitized solar cells^{28,29} and exhibited quite good performances. The commonalities and differences between the crystal structure of BSO and CH₃NH₃PbI₃ (MAPbI₃), which is a classic light harvester in PSCs, are shown in Fig. 1. BSO has the same perovskite structure as the light harvester which might produce a more efficient interface. However, as far as we know, BSO hasn't been employed as electron transporting layer in PSCs.

Herein, we report the first use of mesoporous BSO (mp-BSO) as the mesoporous electron-transporting layer in PSCs. It has a higher electron mobility than TiO₂ and the same structure as CH₃NH₃PbX₃ might to promote electron transport. The effect

^a Key Laboratory of Novel Thin-Film Solar Cells, Institute of Applied Technology, Chinese Academy of Sciences, Hefei 230031, China.
E-mail: xpan@rntek.cas.cn

^b University of Science and Technology of China, Hefei 230026, China.

^c State Key Laboratory of Alternate Electrical Power System with Renewable Energy Sources, North China Electric Power University, Beijing 102206, China
E-mail: sydai@ipp.ac.cn

†Electronic Supplementary Information (ESI) available: Full experimental procedures, UV-vis absorption spectra and XRD patterns of BaSnO₃/MAPbI₃ films and detailed device parameters for optimizing the thickness of BaSnO₃ layer. See DOI: 10.1039/x0xx00000x

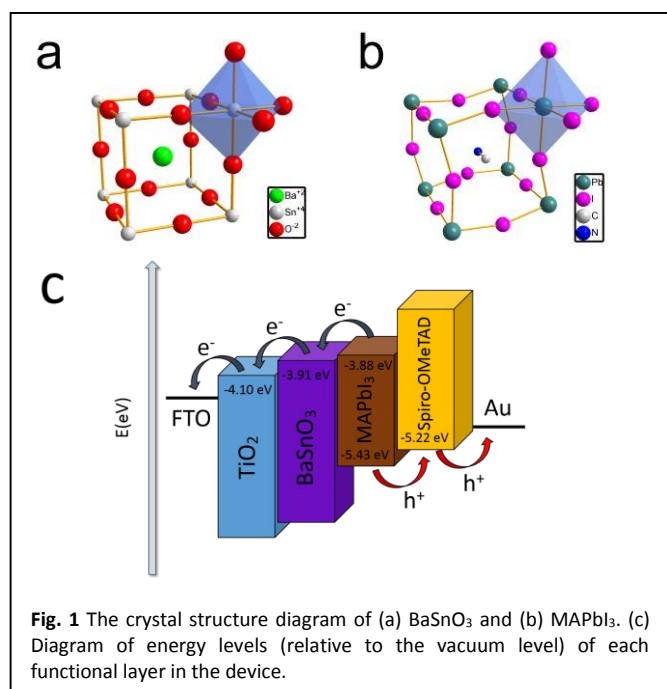


Fig. 1 The crystal structure diagram of (a) BaSnO₃ and (b) MAPbI₃. (c) Diagram of energy levels (relative to the vacuum level) of each functional layer in the device.

of the mp-BSO layers have been investigated and compared with the conventional mesoporous TiO₂ (mp-TiO₂) based device.

The electronic band structure calculated from a literature confirms that perovskite BSO is an indirect band gap semiconductor and has a large band gap of 3.1 eV by experiment test³⁰ which is coincident with the UV-vis absorption spectra (Fig. S1a, ESI[†]). In a direct band gap semiconductor, electrons in conduction band could fall into valence band without a change of momentum, which means the recombination of hole-electron could be quite easy, namely the direct recombination. Different from the direct band gap TiO₂, electrons in the conduction band of BSO are more difficult to fall or recombine. Fig. 1c presents the estimated energy levels (relative to the vacuum level) of each functional layer in the device. The energy level of BSO matches well with other layers lowering the driving force needed for electron injection from MAPbI₃ to BSO.

The synthesis of BaSnO₃ nanoparticles was consulted a method of a literature.²⁸ The crystallinity of nanoparticles could have a deep influence on charge transport in devices. The scanning electron microscopy (SEM) image and transmission electron microscopy (TEM) image of the BSO nanoparticles are shown in Fig. 2a,b. The particle size distribution is relatively concentrated in a small area. The crystallinity and purity of BSO nanoparticles were also characterized in detail by X-ray diffraction (XRD), as shown in Fig. 2c. The crystal structure of BSO obtained from XRD is compared with MAPbI₃ as given in a literature.³¹ As shown in Fig. 1a,b, both BSO and MAPbI₃ have the ABX₃ perovskite structures, which are different from anatase or rutile TiO₂. The stability and geometric distortion of a perovskite ABX₃ structure can be estimated based on the Goldschmidt tolerance factor (t), $t = (r_A + r_X) / [\sqrt{2}(r_B + r_X)]$, where r_A , r_B and r_X are the effective ionic radii for A, B and X ions, respectively. The closer the tolerance factor is from unity, the less distorted the structure will be. The t of BSO is 1.01³² which makes it almost an ideal cubic phase with little distortion and high stability. In contrast, the t of MAPbI₃ is 0.83,³³ deviates from 1 and makes it a tetragonal phase structure.

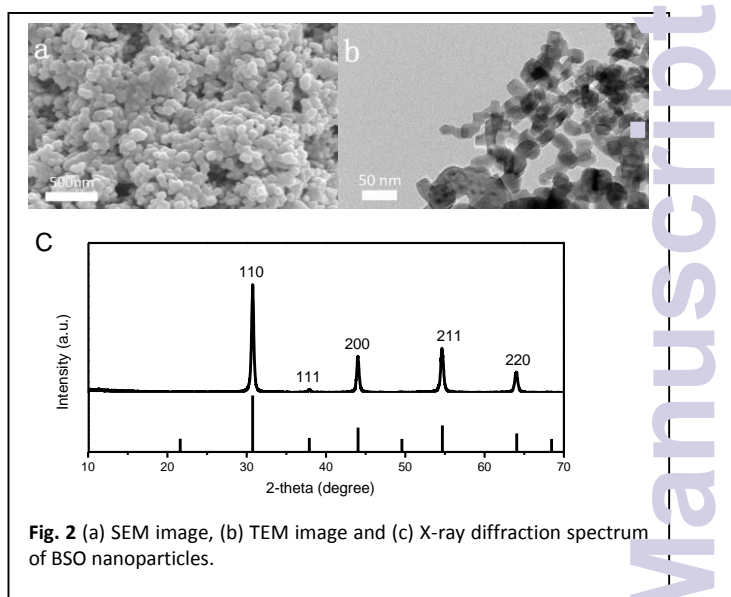


Fig. 2 (a) SEM image, (b) TEM image and (c) X-ray diffraction spectrum of BSO nanoparticles.

In Fig. 3a,b, it can be observed that both mesoporous BSO and TiO₂ based PSCs have a good surface coverage with MAPbI₃ capping layer. The films are well crystallized and there are little voids between crystal boundaries. In contrast, the MAPbI₃ crystals above mp-BSO are more homogeneous than the mp-TiO₂ sample. Greater surface coverage lead to a better overall contact and this would make the MAPbI₃ more uniform. Fig. 3c,d illustrates that BSO has a better contact with MAPbI₃ and makes the crystals grow more unity. The cross-sectional views of mp-BSO and mp-TiO₂ based PSCs are shown in Fig. 3c,d. These two films have a similar total thickness of about 500 nm. The MAPbI₃ is infiltrated into the mesoporous films very well with almost 100% surface coverage above the mesoporous layer, which is coincident with the results of Fig. 3a,b. However, by comparing the mesoporous/MAPbI₃ layers, it can be seen that the interfaces between mp-TiO₂ and MAPbI₃ are more obvious in the mp-TiO₂ film. The mp-BSO/MAPbI₃ film has less crystal boundaries or grainy textures and this will reduce the energy loss and result in lower interface resistance.⁷ The XRD (Fig. S2, ESI[†]) spectra confirm the basic component and indicate that our films remain a part of unreacted PbI₂. A previous research³⁴ has indicated that devices containing PbI₂ can slow down the recombination rate and increase the lifetime of charge carriers by a passivation effect.

To further optimize and study the performance of mp-BSO based PSCs, a series of experiments to optimize the thickness of mp-BSO layer have been done. The thicknesses of mp-BSO layer

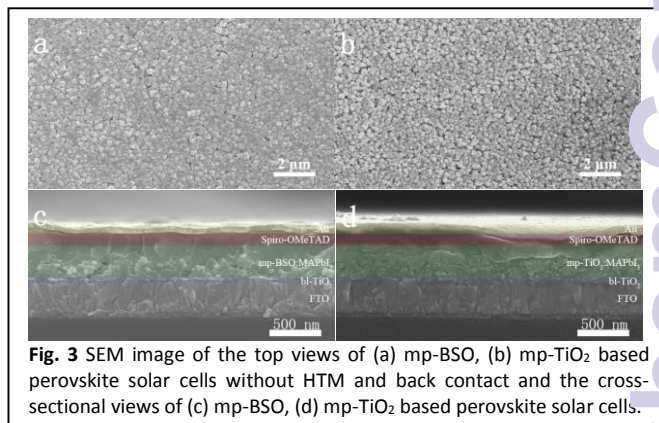


Fig. 3 SEM image of the top views of (a) mp-BSO, (b) mp-TiO₂ based perovskite solar cells without HTM and back contact and the cross-sectional views of (c) mp-BSO, (d) mp-TiO₂ based perovskite solar cells.

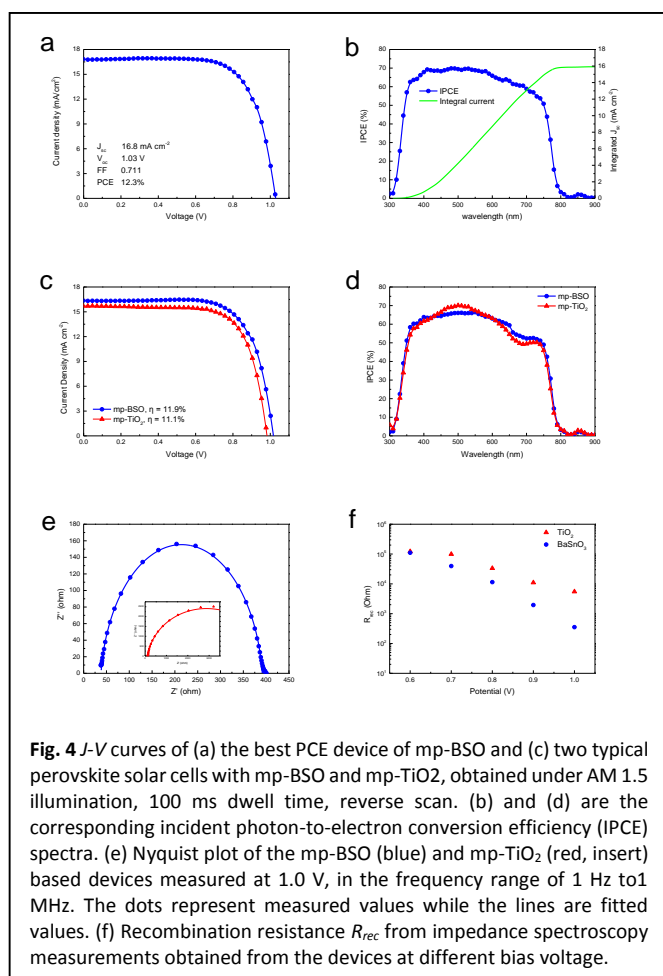


Fig. 4 *J-V* curves of (a) the best PCE device of mp-BSO and (c) two typical perovskite solar cells with mp-BSO and mp-TiO₂, obtained under AM 1.5 illumination, 100 ms dwell time, reverse scan. (b) and (d) are the corresponding incident photon-to-electron conversion efficiency (IPCE) spectra. (e) Nyquist plot of the mp-BSO (blue) and mp-TiO₂ (red, insert) based devices measured at 1.0 V, in the frequency range of 1 Hz to 1 MHz. The dots represent measured values while the lines are fitted values. (f) Recombination resistance R_{rec} from impedance spectroscopy measurements obtained from the devices at different bias voltage.

are between 360 nm and 220 nm, which are controlled by changing the spin-coating speed and measured by cross-sectional SEM images (Fig. S3, ESI[†]). The average values with standard deviation for PCE, short-circuit current density J_{sc} , open-circuit voltage V_{oc} and fill factor (FF) are given in Table 1. (Each group contains 8 samples, detailed device parameters are shown in Table S1.) The highest PCE of 12.3% was achieved using a spin-coating speed of 2000 r.p.m., yielding a J_{sc} of 16.8 mA cm⁻², V_{oc} of 1.03 V, and FF of 0.711 (Fig. 4a,b). The integrated J_{sc} from incident photon-to-electron conversion efficiency (IPCE) data is 15.9 mA cm⁻², agrees with the measured value. The hysteresis of the devices was examined by changing the scan direction in the *J-V* measurements (Fig. S4, ESI[†]). However, the mp-BSO based device exhibited quite large hysteresis which was mainly reflected in the differences in fill factor. Many possible causes have been proposed, such as ferroelectric polarization, charge trapping and ion migration,^{35–37} but there is still no consensus reached at this point. To our knowledge, the hysteresis effect should be related to the nature of the perovskite light harvesting materials and mainly occurs in planar structures. In our cases, such large hysteresis in mesoporous structure is quite unique and rarely reported. Thus a further investigation is needed on this phenomenon.

To compare the PCE of mp-BSO and mp-TiO₂ based PSCs, both devices were fabricated in a similar two-step procedure without TiCl₄ treatment on the mesoporous films. Each group contains 8 samples, detailed device parameters are shown in Table S2 (ESI[†]). The detailed experimental procedures are shown in the experimental section. *J-V* curves and IPCE spectra

Table 1 Mean values with standard deviation (STDEV) of PCE, short-circuit current density J_{sc} , open-circuit voltage V_{oc} and fill factor (FF) based on the thickness of mp-BSO layer, controlled by changing the spin-coating speed from 1000 r.p.m. to 6000 r.p.m. with corresponding accelerations from 1000 r.p.m. s⁻¹ to 6000 r.p.m. s⁻¹. Each group contains 8 samples.

Thickness (nm)	PCE (%)	J_{sc} (mA cm ⁻²)	V_{oc} (V)	FF
385	8.8 ± 2.2	15.2 ± 1.9	0.96 ± 0.05	0.59 ± 0.07
326	11.5 ± 0.7	16.5 ± 0.2	1.02 ± 0.01	0.68 ± 0.03
285	10.2 ± 0.8	14.7 ± 0.9	1.00 ± 0.02	0.69 ± 0.03
253	11.0 ± 0.5	15.4 ± 0.5	1.01 ± 0.01	0.71 ± 0.02
244	10.4 ± 0.6	14.5 ± 0.8	1.01 ± 0.02	0.71 ± 0.02
226	11.0 ± 0.4	14.7 ± 0.5	1.01 ± 0.01	0.74 ± 0.02

of typical mp-BSO and mp-TiO₂ based PSCs are presented in Fig. 4c,d. The *J-V* curves show that mp-BSO device can perform as well as the mp-TiO₂ one and even better. The J_{sc} , V_{oc} and FF of mp-BSO and mp-TiO₂ based devices are 16.3 mA cm⁻², 1.02 V, 0.714 and 15.7 mA cm⁻², 0.98 V, 0.716, respectively. The difference of J_{sc} between two cases can be attributed to the relatively higher electron mobility of BSO. However, the difference is not significant enough. There are three possible reasons: For the first, the whole device based on mp-BSO still remains bi-TiO₂, which has a lower electron mobility and can slow down the entire charge carrier transport. The second, from the normalized UV-vis absorption spectra (Fig. S1b, ESI[†]), it can be seen that the absorption of BSO/MAPbI₃ film is lower than mp-TiO₂/MAPbI₃ film, which can also decrease the J_{sc} . The third, higher electron mobility can increase the J_{sc} and carrier recombination at the same time. The BSO layer exhibited a conduction band minimum (CBM) of 3.91 eV, which is close to the CBM of MAPbI₃. It can make charge carrier “fall back” to MAPbI₃ easier and increase carrier recombination. Meanwhile, the relatively close CBM can also lower the driving force for electron injection, which makes the V_{oc} of mp-BSO device higher than mp-TiO₂ one. The IPCE of the mp-BSO device is lower in the short-wavelength region between 400 nm - 600 nm, which can be attributed to the relatively lower UV-vis absorption in this wavelength region (shown in Fig. S1b, ESI[†]). There is no significant difference of UV-vis absorption between mp-BSO and mp-TiO₂ films in the long-wavelength region between 600 nm and 800 nm, while mp-BSO device exhibited a better IPCE performance in this region.

Electrochemical impedance spectroscopy (EIS) was employed to study the charge transport and recombination in devices (Fig. 4e,f). Comparing the Nyquist plot of the mp-BSO and mp-TiO₂ based devices measured at 1.0 V, the recombination resistance (R_{rec}) of the former one is much smaller. Under low bias voltage, mp-BSO and mp-TiO₂ based devices have the same order of magnitude of R_{rec} . They tend to decrease when bias voltage increased, but the mp-BSO one decreased more. High electron concentration in a semiconductor would cause a higher rate of carrier recombination.³⁸ The data implies that the mp-BSO based devices have almost the same charge recombination rate with mp-TiO₂ under low bias voltage. However, when the carrier concentration is increased by higher bias voltage, the

charge recombination rate of mp-BSO based devices grows much faster than the mp-TiO₂ one. The carrier concentration is also increased by mobility, which means the mp-BSO with a higher electron mobility will have a higher carrier concentration compared with the mp-TiO₂ one under same bias voltage. The relatively close CBM of mp-BSO and MAPbI₃ layers is also an influencing factor for the higher carrier concentration. However, the high electron mobility can increase the charge transport either, the devices still performed well in PCE.

In summary, we have used a novel perovskite oxide, the mp-BSO, as the mesoporous electron-transporting layer in PSCs. As a result, devices based on mp-BSO gave the best performance of 12.3%. Better surface coverage lead to a better overall contact, BSO has a better contact with MAPbI₃ and makes the crystals grow more unity. The high electron mobility of BSO allows an efficient charge collection and contributes to the increase in J_{sc} . And the large band gap can avoid the light absorption competition between BSO and MAPbI₃. The comparison between mp-BSO and mp-TiO₂ based devices showed that mp-BSO device could perform comparatively to the mp-TiO₂ one. However, it also has some issues in the new mp-BSO based device. For example, it has higher charge recombination rate under high bias voltage. The new mp-BSO based PSCs will be a competitive candidate by further optimizing the fabrication procedure and conquering these issues.

This work was financially supported by the National High Technology Research and Development Program of China under Grant no. 2015AA050602, the National Natural Science Foundation of China (Grant no. 61204075) the National Natural Science Foundation of China (Grant no. 21273242).

Notes and references

- A. Kojima, K. Teshima, Y. Shirai, T. Miyasaka, *J. Am. Chem. Soc.*, 2009, **131**, 6050.
- H.-S. Kim, C.-R. Lee, J.-H. Im, K.-B. Lee, T. Moehl, A. Marchioro, S.-J. Moon, R. Humphry-Baker, J.-H. Yum, J. E. Moser, M. Grätzel, N.-G. Park, *Sci. Rep.*, 2012, **2**, 591.
- M. M. Lee, J. Teuscher, T. Miyasaka, T. N. Murakami, H. J. Snaith, *Science*, 2012, **338**, 643.
- J. Burschka, N. Pellet, S. J. Moon, R. Humphry-Baker, P. Gao, M. K. Nazeeruddin, M. Grätzel, *Nature*, 2013, **499**, 316.
- Chen, H.; Pan, X.; Liu, W.; Cai, M.; Kou, D.; Huo, Z.; Fang, X.; Dai, S., *Chem. Commun.*, 2013, **49**, 7277.
- H. Zhou, Q. Chen, G. Li, S. Luo, T.-b. Song, H.-S. Duan, Z. Hong, J. You, Y. Liu, Y. Yang, *Science*, 2014, **345**, 542.
- J. H. Im, I. H. Jang, N. Pellet, M. Grätzel, N. G. Park, *Nat. Nanotech.*, 2014, **9**, 927.
- N. J. Jeon, J. H. Noh, W. S. Yang, Y. C. Kim, S. Ryu, J. Seo, S. I. Seok, *Nature*, 2015, **517**, 476.
- J. W. Lee, D. J. Seol, A. N. Cho, N. G. Park, *Adv. Mater.*, 2014, **26**, 4991.
- Z. Xiao, Q. Dong, C. Bi, Y. Shao, Y. Yuan, J. Huang, *Adv. Mater.*, 2014, **26**, 6503.
- W. S. Yang, J. H. Noh, N. J. Jeon, Y. C. Kim, S. Ryu, J. Seo, S. I. Seok, *Science*, 2015, **348**, 1234.
- H. S. Jung, N. G. Park, *Small*, 2015, **11**, 10.
- M. Grätzel, *Nature*, 2001, **414**, 338.
- J.-W. Lee, T.-Y. Lee, P. J. Yoo, M. Grätzel, S. Mhaisalkar, N.-G. Park, *J. Mater. Chem. A*, 2014, **2**, 9251.
- Matthew J. Carnie, Cecile Charbonneau, Matthew L. Davies, Joel Troughton, Trystan M. Watson, Konrad Wojciechowski, Henry Snaith, David A. Worsley, *Chem. Commun.*, 2013, **4**, 7893.
- Matthew J. Carnie, Cecile Charbonneau, Matthew L. Davies, Brian O' Regan, David A. Worsley, Trystan M. Watson, *J. Mater. Chem. A*, 2014, **2**, 17077.
- Q. Zhang, C. S. Dandeneau, X. Zhou, G. Cao, *Adv. Mater.*, 2009, **21**, 4087.
- M. H. Kumar, N. Yantara, S. Dharani, M. Graetzel, S. Mhaisalkar, P. P. Boix, N. Mathews, *Chem. Commun.*, 2013, **4**, 11089.
- D.-Y. Son, J.-H. Im, H.-S. Kim, N.-G. Park, *J. Phys. Chem. C*, 2014, **118**, 16567.
- J. Zhang, P. Barboux, T. Pauporté, *Adv. Energy Mater.*, 2014, **4**, 1400932.
- L. S. Oh, D. H. Kim, J. A. Lee, S. S. Shin, J.-W. Lee, I. J. Park, M. J. Ko, N.-G. Park, S. G. Pyo, K. S. Hong, J. Y. Kim, *J. Phys. Chem. C*, 2014, **118**, 22991.
- S. S. Mali, C. Su Shim, C. Kook Hong, *Sci. Rep.*, 2015, **5**, 11474.
- S. S. Shin, W. S. Yang, J. H. Noh, J. H. Suk, N. J. Jeon, J. H. Park, J. S. Kim, W. M. Seong, S. I. Seok, *Nat. Commun.*, 2015, **6**, 7410.
- A. Bera, K. Wu, A. Sheikh, E. Alarousu, O. F. Mohammed, J. Wu, *J. Phys. Chem. C*, 2014, **118**, 28494.
- J. T.-W. Wang, J. M. Ball, E. M. Barea, A. Abate, J. A. Alexander-Webber, J. Huang, M. Saliba, I. Mora-Sero, J. Bisquert, H. Snaith, R. J. Nicholas, *Nano Lett.*, 2014, **14**, 724.
- C. Park, U. Kim, C. J. Ju, J. S. Park, Y. M. Kim, K. Char, *Appl. Phys. Lett.*, 2014, **105**, 203503.
- H. J. Kim, U. Kim, H. M. Kim, T. H. Kim, H. S. Mun, B.-G. Jeon, K. T. Hong, W.-J. Lee, C. Ju, K. H. Kim, K. Char, *Appl. Phys. Express*, 2012, **5**, 061102.
- D. W. Kim, S. S. Shin, S. Lee, I. S. Cho, D. H. Kim, C. W. Lee, H. S. Jung, K. S. Hong, *ChemSusChem*, 2013, **6**, 449.
- S. S. Shin, J. S. Kim, J. H. Suk, K. D. Lee, D. W. Kim, J. H. Park, I. S. Cho, K. S. Hong, J. Y. Kim, *ACS Nano*, 2013, **7**, 1027.
- E. Moreira, J. M. Henriques, D. L. Azevedo, E. W. S. Caetano, V. N. Freire, U. L. Fulco, E. L. Albuquerque, *J. Appl. Phys.*, 2011, **112**, 043703.
- C. C. Stoumpos, C. D. Malliakas, M. G. Kanatzidis, *Inorg. Chem.*, 2013, **52**, 9019.
- W. Zhang, J. Tang, J. Ye, *J. Mater. Res.*, 2007, **22**, 1859.
- N.-G. Park, *Mater. Today*, 2015, **18**, 65.
- L. Wang, C. McCleese, A. Kovalsky, Y. Zhao, C. Burda, *J. Am. Chem. Soc.*, 2014, **136**, 12205.
- J. Wei, Y. Zhao, H. Li, G. Li, J. Pan, D. Xu, Q. Zhao, D. Yu, *J. Phys. Chem. Lett.*, 2014, **5**, 3937.
- Y. Shao, Z. Xiao, C. Bi, Y. Yuan, J. Huang, *Nat. Commun.*, 2011, **5**, 5784.
- Z. Xiao, Y. Yuan, Y. Shao, Q. Wang, Q. Dong, C. Bi, P. Sharma, A. Gruverman, J. Huang, *Nat. Mater.*, 2015, **14**, 193.
- D. H. Kim, G. S. Han, W. M. Seong, J.-W. Lee, B. J. Kim, N.-G. Park, K. S. Hong, S. Lee, H. S. Jung, *ChemSusChem*, DOI: 10.1002/cssc.201403478.